Part II

Energy Minimisation Simulation of Bulk Materials

"What has mood to do with it?

You fight when the necessity arises–no matter the mood!

Mood's a thing for cattle or making love or playing the baliset.

It's not for fighting."

–the words of Gurney Halleck

Chapter 3

Methodology Associated with Energy Minimisation

3.1 Bulk Lattice Simulation Detail

The initial phase of any lattice simulation is to evaluate the lattice energy, U_L, of the system. At the same time physical properties can be found from the first and second derivatives of the lattice energy with respect to interatomic separation. The accuracy of this data compared to experimentally derived results provide a means of verifying the model parameters. Here the lattice energy is found by summation of the energy contribution from all ion pair interactions,

$$U_L = \frac{1}{2}\sum_{i=1}^{n}\sum_{i\neq j}^{n}\Phi_{ij}(r_{ij}) \tag{3.1}$$

where $\Phi_{ij}(r_{ij})$ is the two body interaction energy $(\Phi_{lr}(r_{ij})+\Phi_{sr}(r_{ij}))$ and n is the number of atoms in the system. Note the term $\frac{1}{2}$ is due to a double counting of interactions. Self interactions are also avoided in the summation. With reference to chapter 2, the mathematical form of $\Phi_{lr}(r_{ij})$ is equation 2.3 and $\Phi_{sr}(r_{ij})$ can be any of 2.4-2.9. Due to its previously mentioned success the Buckingham potential is used for polarisable ions in

this work and less polarisable cations are modelled with the Born-Mayer potential. Thus, expanding 3.1,

$$U_L = \frac{1}{2}\sum_{i=1}^{n}\sum_{i\neq j}^{n}\left[\frac{q_i q_j}{4\pi\varepsilon_0 r_{ij}} + A_{ij}\, exp\left(\frac{-r_{ij}}{\rho_{ij}}\right) - \frac{C_{ij}}{r_{ij}^6}\right] \tag{3.2}$$

As the number of atoms in the system increases the solution of equation 3.1 tends toward the lattice energy. Herein lies a computational problem. Since the coulombic interaction operates over a long range, the evaluation of such a large number of coulombic interactions is computationally expensive. While this can be overcome with more powerful computers and series approximation mathematics, the computation is further complicated since the order in which the summation is performed influences the final result. No such problem is encountered with the short range term as it is truncated at approximately 20Å. This convergence issue, for the long range term, is overcome by applying the method due to Ewald [18].

3.1.1 Ewald Summation

The Ewald method calculates the electrostatic potential acting on a object ion, i, in a lattice. The lattice is made up of ions acting as an array of positive and negative charge points. The total potential, ϕ, acting on the object ion by the array of point charges is separated into two components. One part in real space, ϕ_1, and the other in reciprocal space, ϕ_2, such that,

$$\phi = \phi_1 + \phi_2 \tag{3.3}$$

The real part, ϕ_1, comprised of the array of point charges is countered by an array of Gaussian charge distributions equivalent in magnitude but opposite in charges (see figure 3.1). Thus, each ion is effectively neutralised and neighbouring ions no longer interact.

The reciprocal part, ϕ_2, comprises an array of Gaussian charge distributions, ϕ_L, with equivalent charge and magnitude as the original point charge array. However, since in

a Madelung array of ions individual ions do not feel their own electrostatic field, the charge distribution of the object ion, ϕ_i, is removed from the reciprocal part (see equation 3.4 and figure 3.2).

$$\phi_2 = \phi_L - \phi_i \tag{3.4}$$

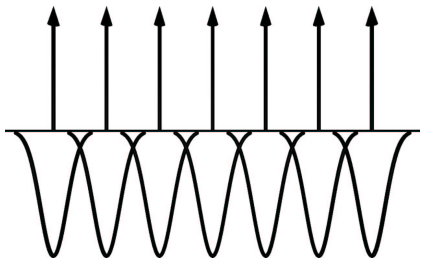

Figure 3.1: Graphical representation of ϕ_1 in a 1-dimensional lattice. Arrows represent point charges which are countered by Gaussian charge distributions of equivalent magnitude but opposite charge.

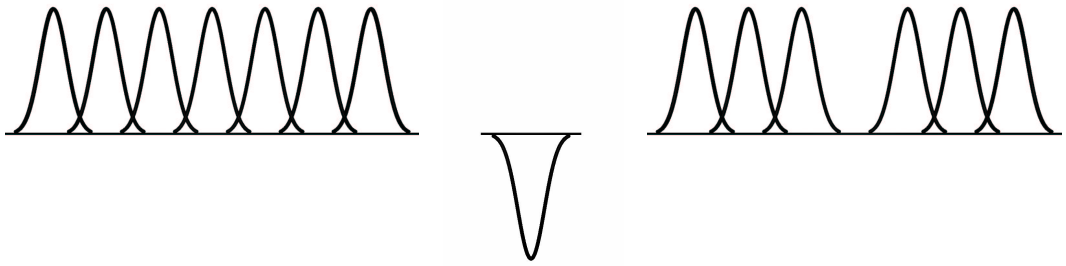

(a) ϕ_L (b) $-\phi_i$ (c) $\phi_L - \phi_i = \phi_2$

Figure 3.2: Graphical representation of the construction of ϕ_2 in a 1-dimensional lattice: a) array of Gaussian distributions, ϕ_L, b) oppositely charged Gaussian distribution of the object ion, $-\phi_i$, c) combined effect ($\phi_L - \phi_i$) whereby the object ion does not feel its own electrostatic field.

When ϕ_1 and ϕ_2 are combined, the Gaussian charge distributions cancel and the overall potential of the array is reduced to that of the original point charge array. The

purpose of the Gaussian distributions is to create smoothly varying functions which converge rapidly. This benefits the summation such that rapid convergence of ϕ_1 and ϕ_2 (and therefore ϕ) can be achieved.

Potential ϕ_1, evaluated at the object ion, has three components: the point charge associated with the object ion, the Gaussian distribution within a sphere of radius r_{ij} (distance to the nearest neighbour of the object ion) and the Gaussian distribution of the object ion outside the sphere. For an object ion interacting with a lattice of ion, j, the real part of the potential has the form,

$$\phi_1 = \frac{q_j}{4\pi\varepsilon_0} \sum_i \frac{q_i}{r_{ij}} erfc(\eta^{\frac{1}{2}} r_{ij}) \tag{3.5}$$

where $erfc$ is the complimentary error function which is related to the standard error function, $erf(x)$, by,

$$erfc(x) = 1 - erf(x) \tag{3.6}$$

and η is a variable parameter chosen to maximise the efficiency of the convergence.

A Fourier transformation is applied to ϕ_2 so that it converges rapidly in reciprocal space. Since the system is periodic (i.e. a lattice) ϕ_L and its charge density θ can be expressed as Fourier series:

$$\phi_L = \sum_G c_G \, exp \, \mathbf{i}(\mathbf{G} \cdot \mathbf{r}) \tag{3.7}$$

and

$$\theta = \sum_G \theta_G \, exp \, \mathbf{i}(\mathbf{G} \cdot \mathbf{r}) \tag{3.8}$$

where c_G and θ_G are coefficients and $\mathbf{G}$ is 2π times the set of reciprocal lattice vectors. The series converge as $\mathbf{G}$ increases and the coefficients decrease. The electrostatic potential is related to the charge density by Poisson's equation,

$$\nabla^2 \phi_L = -\frac{\theta}{\varepsilon_0} \tag{3.9}$$

Using equation 3.9, ϕ_L can be rewritten,

$$\phi_L = q_j \sum_i \left[q_i \frac{4\pi}{V_C} \sum_G \left(\frac{1}{G^2} exp - \left(\frac{G^2}{4\eta} \right) exp - \mathbf{i}(\mathbf{G} \cdot \mathbf{r}) \right) \right] \tag{3.10}$$

where V_C is the unit cell volume. Note if $\mathbf{G} = 0$ then $\phi \Rightarrow \infty$. However, since the sum of charges in a unit cell, $\mathbf{i}$, is assumed to be zero, then the whole of the last term can be ignored when $\mathbf{G} = 0$.

The potential ϕ_i at the subject ion due to the Gaussian distribution is,

$$\phi_i = \frac{2q_i^2}{\varepsilon_0} \left(\frac{\eta}{\pi} \right)^{\frac{1}{2}} \tag{3.11}$$

and substitution of equations 3.10 and 3.11 into equation 3.4 gives,

$$\phi_2 = q_j \sum_i \left[q_i \frac{4\pi}{V_C} \sum_G \left(\frac{1}{G^2} exp - \left(\frac{G^2}{4\eta} \right) exp - \mathbf{i}(\mathbf{G} \cdot \mathbf{r}) \right) \right] - \frac{2q_i^2}{\varepsilon_0} \left(\frac{\eta}{\pi} \right)^{\frac{1}{2}} \tag{3.12}$$

Finally, substituting equations 3.5 and 3.12 into equation 3.3 provides an expression for the overall coulombic interaction that can be used to obtain the lattice energy.

$$\begin{aligned} \phi = & \frac{q_j}{4\pi\varepsilon_0} \sum_i \frac{q_i}{r_{ij}} erfc(\eta^{\frac{1}{2}} r_{ij}) \\ & + q_j \sum_i \left[q_i \frac{4\pi}{V_C} \sum_G \left(\frac{1}{G^2} exp - \left(\frac{G^2}{4\eta} \right) exp - \mathbf{i}(\mathbf{G} \cdot \mathbf{r}) \right) \right] \\ & - \frac{2q_i^2}{\varepsilon_0} \left(\frac{\eta}{\pi} \right)^{\frac{1}{2}} \end{aligned} \tag{3.13}$$

It is possible to choose a value for η which will make the Fourier expansion fall off rapidly and at the same time make the sum of the potentials of the Gaussians converge conveniently [19].

3.1.2 Energy Minimisation

If potentials precisely reproduce the force field surrounding the ions then the lattice energy of the simulated crystal will be at a minimum when ionic distances exactly match the

observed crystal structure. However, this is rarely achievable since potentials are a simple representation of a more complex distribution of forces. Nevertheless, such potentials do provide sensible results. In practise the lattice is always relaxed until it reaches a minimum energy configuration where, even though there may be some error from the observed structure, lattice strains are minimised. It is of course essential that the relaxed configuration of the simulation is as close as possible to the observed crystal lattice. In this way the response of the simulated lattice to point defects will be representative of the response of the real lattice.

The system is minimised by iteratively adjusting the coordinates of ions until the forces on the atoms are zero,

$$\frac{\partial U_L}{\partial r} = 0 \tag{3.14}$$

where U_L is the lattice energy and r is the coordinate system. The term zero force is used since the derivative of lattice energy with respect to distance is force. This point will become useful when the calculation of elastic properties of a lattice are discussed.

Following the method laid out by Catlow and Norgett [20] (more recently detailed by Catlow and Macrodt [21]), if the lattice energy of a system with coordinates, r, is $U_L(r)$ then the lattice energy at a new set of coordinates r' is,

$$U_L(r') = U_L(r) + \underline{g}^T \cdot \underline{\delta} + \frac{1}{2}\underline{\delta}^T \cdot \mathbf{W} \cdot \underline{\delta} \tag{3.15}$$

where $\underline{\delta}$ is a generalised strain vector with 3N orthogonal displacement components, $\underline{\delta r}$, and 6 bulk strain components, $\underline{\delta\varepsilon}$. Thus,

$$\underline{\delta} = (\underline{\delta r}, \underline{\delta\varepsilon}) \tag{3.16}$$

The vector $\underline{g}$ corresponds to the first derivatives of the lattice energy with respect to the ion displacements and strain components,

$$\underline{g} = \left(\frac{\partial U_L}{\partial \underline{r}}, \frac{\partial U_L}{\partial \underline{\varepsilon}}\right) \tag{3.17}$$

and $\mathbf{W}$ is the second derivative matrix,

$$\mathbf{W} = \begin{pmatrix} \frac{\partial^2 U}{\partial r \partial r} & \frac{\partial^2 U}{\partial r \partial \varepsilon} \\ \frac{\partial^2 U}{\partial \varepsilon \partial r} & \frac{\partial^2 U}{\partial \varepsilon \partial \varepsilon} \end{pmatrix} \tag{3.18}$$

The new coordinates r' are related to the original coordinates by,

$$r' = \Delta\varepsilon(r + \delta r) \tag{3.19}$$

where $\Delta\varepsilon$ is the Voight matrix representation of the vector $\underline{\delta\varepsilon}$,

$$\Delta\varepsilon = \begin{pmatrix} \delta\varepsilon_1 & \frac{1}{2}\delta\varepsilon_6 & \frac{1}{2}\delta\varepsilon_5 \\ \frac{1}{2}\delta\varepsilon_6 & \delta\varepsilon_2 & \frac{1}{2}\delta\varepsilon_4 \\ \frac{1}{2}\delta\varepsilon_5 & \frac{1}{2}\delta\varepsilon_4 & \delta\varepsilon_3 \end{pmatrix} \tag{3.20}$$

The lattice energy may be minimised by allowing the ion coordinates to change in a way that reduces the lattice strain. Energy may be minimised with respect to internal unit cell ion coordinates (i.e. under constant volume conditions). Alternatively, the strain on the cell vectors may also be minimised (i.e under constant pressure conditions).

To minimise the lattice energy under constant volume differentiate equation 3.15, with respect to the coordinate system. This is analogous to saying energy, $\mathbf{E}$, can be expressed as force, $\mathbf{F}$, times distance, $\mathbf{d}$; where the differential, with respect to distance, is force:

$$\mathbf{E} = \mathbf{F} \times \mathbf{d} \tag{3.21}$$

$$\frac{\partial \mathbf{E}}{\partial \mathbf{d}} = \mathbf{F} \tag{3.22}$$

Thus in the case of a lattice where the forces are zero:

$$\begin{aligned} \therefore \frac{\partial U_L(r')}{\partial r} &= 0 \\ &= \frac{\partial U_L(r)}{\partial r} + \frac{\partial g^T}{\partial r} \cdot \delta \qquad &= 0 \\ &= g + \mathbf{W}\delta \qquad &= 0 \end{aligned} \tag{3.23}$$

Which leads to a minimum in lattice energy, and zero force, when

$$g = -\mathbf{W}\delta \tag{3.24}$$

and the optimum ion displacements to give the minimum energy are:

$$\delta = -\mathbf{W}^{-1}g \tag{3.25}$$

Thus, new lattice coordinates can be found.

To proceed onto a constant pressure calculation the bulk strains are also minimised by relaxation of the cell vectors. Bulk strains are defined such that they transform every vector r in the lattice to r' where,

$$r' = (\mathbf{I} + \varepsilon) \cdot r \tag{3.26}$$

where $\mathbf{I}$ is the identity matrix and ε is the symmetric strain tensor related to equation 3.20. Thus, equations 3.26 and 3.19 can be combined to give the new lattice vectors and coordinates.

There are several minimisation procedures that can be applied, of which the Newton-Raphson method is commonly implemented. In this procedure the value of r at the $(n+1)$ iteration is related to the nth iteration by,

$$r_{n+1} = r_n - \mathbf{W}_n^{-1} \cdot g_n \tag{3.27}$$

3.1.3 Calculation of Physical Properties

In a similar manner to differentiating with respect to ion displacement the first derivative of the lattice energy with respect to strain is the stress, σ. Applying Hooke's law, the elastic constant matrix can be defined.

$$\frac{\partial U_L}{\partial \delta\varepsilon} = \sigma \tag{3.28}$$

$$\sigma = \mathbf{C}\,\varepsilon \tag{3.29}$$

$$\frac{\partial U_L}{\partial \delta\varepsilon} = \mathbf{C}\,\delta\varepsilon \tag{3.30}$$

where $\mathbf{C}$ is the elastic constant matrix. Taking the second derivative of lattice energy with respect to strain, the elastic constant matrix becomes immediately accessible,

$$\frac{\partial^2 U_L}{\partial \delta\varepsilon^2} = \mathbf{C} \tag{3.31}$$

3.1.4 Electronic Polarisability

The response of an atoms electron charge density to an electric field is incorporated through the shell model of Dick and Overhausser [22]. In their model ions are described with charge divided between a core and a massless shell, as shown in figure 3.3. The core and shell are coupled by an isotropic harmonic force constant, K. The ion charge is divided between the core, with charge Xe, and the shell, with charge Ye, so that total charge on the ion is $(X+Y)e$. Using this description the electronic polarisability of a free ion, α_e, is

$$\alpha_e = \frac{1}{4\pi\varepsilon_0}\left(\frac{Y^2}{K}\right) \tag{3.32}$$

where K is in units of eVÅ^{-2} and ε_0 is the permittivity of free space.

With this model dipoles are produced by moving the shell relative to the core. The ease of this movement (the polarisability) is controlled by the force constant and the charges on the core and shell. The parameters of the shell model (X, Y and K) are found by empirical fitting to the dielectric and elastic properties of the crystal. Since electronic polarisability is the only factor in the high frequency dielectric constant, ε_∞, it

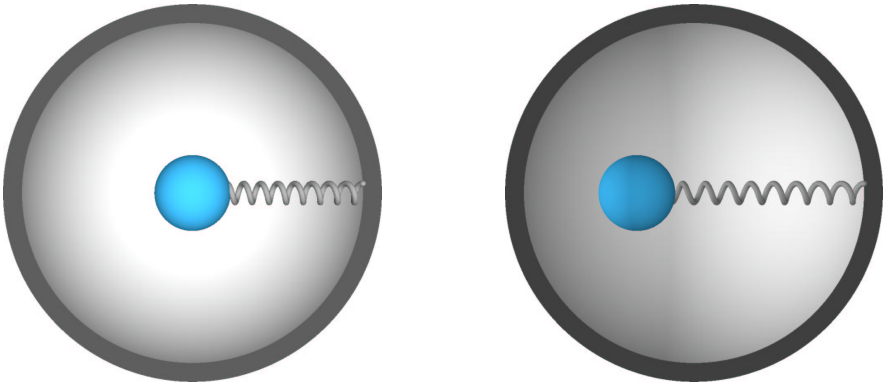

(a) Unpolarised (b) Polarised

Figure 3.3: Graphical representation of the shell model: a) no displacement, unpolarised. b) displacement, polarised. The blue sphere, representing the core, has charge Xe. The open gray sphere, representing the shell, has charge Ye. The core and shell are connected by a spring of force constant K.

is the main fitting observable for the model parameters. The static dielectric constant, ε_s, has a contribution from the ionic polarisation of the lattice, which is only operative at lower frequencies. As such ε_s is the less important fitting observable.

The usefulness of this model is largely due to its coupling of the short range interaction to the polarisability. It is assumed that short range interactions act between shells. In using this treatment a complex model for ion interactions is formed. This leads to a much more complex calculation and some of the simplicity of using two body terms is lost. Naturally this impacts significantly on the computational expense of the simulation.

The shell model is limited, however, since it cannot reproduce the Cauchy violation [23]. In using two-body terms the calculation of elastic constants will always evaluate C_{12} equal to C_{44}, however real materials can violate this. The inflexibility arises due to the use of a fixed radius shell. Techniques have been proposed to correct this issue. By assigning a real radius to the shell and allowing this to change, values of C_{12} greater than C_{44} can be achieved (i.e. positive deviations only). This is known as a breathing shell model [24].

Values of C_{12} less than C_{44} can only be achieved by allowing ellipsoidal shells [25].

3.1.5 Defective Lattice

Once a minimised lattice has been established defects can be introduced. The response of the lattice to defect incorporation will be to reduce the energy of the system by further relaxation of ion coordinates. The majority of the relaxation is assumed to be localised to a volume surrounding the defects. This allows the the application of a multi-region approach where an inner, region I, extends from the centre of the defect site to some predetermined radius. Here interactions are calculated explicitly and all ion displacements are determined. An outer, region II, extends from the edge of region I to infinity. Region II is further sub-divided into region IIa and IIb, where IIa acts as a transition between regions I and II. In region IIa ion displacements and induced moments are inferred from the Mott-Littleton approximation [26] but interactions with ions in region I are calculated by explicit summation. The displacements and induced moments of ions in region IIb are inferred since the total response energy is approximated using the Mott-Littleton equation.

With the Mott-Littleton approximation, the lattice response at distance r, from a defect of charge q is described in terms of the crystal polarisation P,

$$P = \frac{1}{4\pi}\left(1 - \frac{1}{\varepsilon}\right)\frac{q}{r^2} \tag{3.33}$$

where $\varepsilon = \varepsilon_s\varepsilon_0$.

From equation 3.33 individual displacements and electronic moments can be inferred by summing the corresponding interaction over the whole lattice. With reference to figure 3.4 it can be seen that the total energy introduced into the lattice by incorporation of a defect, E_d, is the sum of each part of the multi-region approach,

$$E_d = E_1 + E_2(r) + E_3(r,\zeta) + E_4(\zeta) \tag{3.34}$$

where E_1 is the energy of the defect in an unrelaxed non-polarisable lattice. The response of the lattice is a function of either the atom coordinates in region I, r, or the displacement vector in region II, ζ. E_2 is the energy of region I due to the ion displacements, r. E_3 is the interaction between Region I and II and is a function of r and the displacement vector ζ. E_4 is the energy of region II due to the displacement vector ζ.

Since E_4 is the sum of an infinite number of displacements it cannot be solved exactly but is found by assuming displacements in region II are quasi-harmonic, such that

$$E_4(\zeta) = \frac{1}{2}\zeta \cdot \mathbf{A} \cdot \zeta \tag{3.35}$$

where $\mathbf{A}$ is the force constant matrix. Substituting 3.35 into 3.34 and differentiating with respect to ζ, the displacements in region II at equilibrium are,

$$\left.\frac{\partial E_3(r,\zeta)}{\partial \zeta}\right|_{\zeta=\zeta_e} = -\mathbf{A} \cdot \zeta_e \tag{3.36}$$

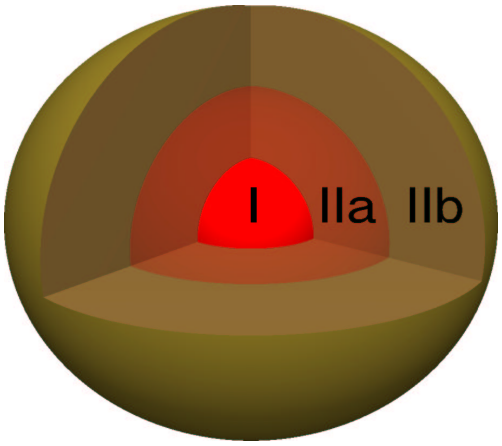

Figure 3.4: Representation of the two region approach for defect energy calculations. The inner region, I, surrounds the defect and ion displacements are calculated explicitly. In the outer region, IIb, displacements are calculated using the Mott-Littleton approximation. Region IIa acts as a transition between Region I and IIb.

thus from equation 3.35,

$$E_4(\zeta) = -\frac{\zeta}{2}\left.\frac{\partial E_3(r,\zeta)}{\partial \zeta}\right|_{\zeta=\zeta_e} \tag{3.37}$$

E_4 can now be removed from equation 3.34 giving,

$$E = E_1 + E_2(r) + E_3(r,\zeta) - \left.\frac{\zeta}{2}\frac{\partial E_3(r,\zeta)}{\partial \zeta}\right|_{\zeta=\zeta_e} \tag{3.38}$$

The radii of regions I and IIa have a direct impact on the accuracy of the calculated defect energy and also the computational effort required to reach a minimum solution. Values are chosen such that further increases do not significantly alter the results obtained. Table 3.1 details the region sizes used for host lattice simulations in chapters 4 and 5.

Table 3.1: Host lattice region I and II sizes used in simulations.

Lattice	Region I (Å)	Region IIa (Å)
NiF_2	10.23	28.83
α-Al_2O_3	12.03	32.51
α-Cr_2O_3	12.57	33.96
α-Fe_2O_3	12.69	34.30

3.2 Derivation of Model Parameters

The derivation of model parameters is critical to any successful simulation. Some model parameters can be derived from mathematical analysis, others are amenable to empirical selection methods. Wherever possible experimental data is used to test the validity of the resulting model. It is important to realise that while some parameters may have a physical meaning (see section 2.2.2 on page 29) this does not have to be absolutely followed. In the case of the interatomic potentials it is also important to remember that potentials are meant to reproduce the total interaction of forces and are not limited to reproducing the ionicity of the bond. Thus this technique is extended into somewhat more covalently bonded systems [27, 28].

3.2.1 Non-empirical Methods

There are several methodologies for arriving at model parameters. These involve empirical or non-empirical techniques. Quantum mechanical cluster calculations can be used to determine parameters for a system [29]. Alternatively the electron gas method can be used which treats the electron density around the ions as a Fermi-gas. Such an approach is implemented in a series of programs by Harding and Harker [30]. To find parameters of a given interaction using the electron gas method, the interaction between ions is approximated by calculating the energies associated with the overlap of the electron gas densities. This is achieved through the method of Wedepohl [31] and Gordon and Kim [32]. Several assumptions are made about the electron density in this approach and are detailed by Gluston [33].

3.2.2 Empirical Methods

Neither of these approaches were used in this work due to the availability of good starting potentials. As such, an empirical approach could be used to develop reliable potentials in a self consistent manner.

Empirical potentials suffer one significant drawback, they only calculate a single point on the potential surface. When defects are simulated, different interatomic separations are encountered and the potential may not correctly reproduce the interaction in over an extended separation range. This limitation can be overcome by fitting a potential to several structures simultaneously. Here this “multi-fitting” approach is used to develop potentials for the NiF_2 system.

3.2.3 Potential Listing for Bulk Lattice Systems

It is vital to the validity of a study that all potentials are self consistent with each other. Full formal charge states are assumed (such that q is an integer), despite the evidence that full charge models with a shell, as implemented here, consistently overestimate reaction energies by approximately 40% [34]. Again this highlights why only relative energies for processes are emphasised and discussed, not absolutes.

Two bulk lattice studies are contained within this work. The first, detailed in chapter 4, studies the nickel fluoride lattice and the incorporation of extrinsic solutes in detail. Short-range potentials were derived specifically for this work and are given in table 3.2. The shell charge for fluorine was -1.3776 $|e|$ and the spring constant was 24.36 eVÅ^{-2}. The second study, detailed in chapter 5, investigates solution of extrinsic defects in α-Al_2O_3, α-Cr_2O_3 and α-Fe_2O_3. Short-range potentials for these oxide systems were taken from the literature and are detailed in table 3.3. The shell charge for oxygen was -2.04 $|e|$ and the spring constant was 6.3 eVÅ^{-2}.

3.3 Ionic Lattice Simulation Techniques

Aside from deriving a set of model parameters that correctly simulate the system under study, there is the conceptual link between simulation and reality. The aim of these simulations is to gain a quantitative description of various point defect processes that are inaccessible by experimentation. Simulations can be used in a variety of ways as described below. For the detailed practicalities of using each code the relevant manuals are recommend.

Table 3.2: Short-range potential parameters used to model defects in the host NiF_2 lattice.

Species	Ionic Radii [35] (Å)	A (eV)	ρ (Å)	C (eVÅ^6)
F^--F^-	1.33	1317.5	0.2753	13.8
Li^+-F^-	0.67	575.8	0.2553	0.0
Na^+-F^-	1.02	1497.45	0.2589	0.0
Ag^+-F^-	1.15	1696.2	0.2699	0.0
K^+-F^-	1.38	1701.31	0.2963	13.7
Rb^+-F^-	1.52	1267.9	0.3219	21.4
Cs^+-F^-	1.67	1758.8	0.3279	32.1
Ni^{2+}-F^-	0.69	907.9	0.2816	0.0
Mg^{2+}-F^-	0.72	841.3	0.2831	0.0
Co^{2+}-F^-	0.745	917.2	0.2856	0.0
Fe^{2+}-F^-	0.78	934.9	0.2879	0.0
Mn^{2+}-F^-	0.83	1000.7	0.2926	0.0
Cd^{2+}-F^-	0.95	1057.6	0.3059	10.0
Ca^{2+}-F^-	1.00	1534.3	0.2893	0.0
Ba^{2+}-F^-	1.35	1746.9	0.3237	16.7
Al^{3+}-F^-	0.535	1409.9	0.2577	0.0
Cr^{3+}-F^-	0.615	1124.7	0.2706	0.0
Fe^{3+}-F^-	0.645	1246.2	0.2788	0.0
Mo^{3+}-F^-	0.69	1436.2	0.2864	12.6
Sc^{3+}-F^-	0.745	1364.7	0.2953	0.0
Y^{3+}-F^-	0.9	2146.3	0.2985	12.4
La^{3+}-F^-	1.032	1384.9	0.3302	16.0

Table 3.3: Short-range potential parameters used to model host corundum oxides lattices (α-Al_2O_3, α-Cr_2O_3 and α-Fe_2O_3) and cation dopants.

Species	ionic Radii [35] (Å)	A (eV)	ρ (Å)	C (eVÅ^6)	Reference
O^{2-}-O^{2-}	1.40	9547.96	0.2192	32.0	[7, 14, 16, 36–39]
Mg^{2+}-O^{2-}	0.72	1248.38	0.299969	0.0	[37]
Co^{2+}-O^{2-}	0.745	778.02	0.3301	0.0	[39]
Fe^{2+}-O^{2-}	0.78	853.5	0.3288	0.0	[14]
Cd^{2+}-O^{2-}	0.95	951.88	0.34856	13.91	[36]
Ca^{2+}-O^{2-}	1.00	784.38	0.36356	0.0	[36]
Sr^{2+}-O^{2-}	1.18	682.17	0.3945	0.0	[38]
Ba^{2+}-O^{2-}	1.35	905.7	0.3976	0.0	[36]
Al^{3+}-O^{2-}	0.535	1120.04	0.3125	0.0	[38]
Cr^{3+}-O^{2-}	0.615	1313.18	0.3165	0.0	[38]
Ga^{3+}-O^{2-}	0.620	1281.75	0.3175	0.0	[38]
Fe^{3+}-O^{2-}	0.645	1414.60	0.3128	0.0	[36]
Sc^{3+}-O^{2-}	0.745	1575.85	0.3211	0.0	[36]
In^{3+}-O^{2-}	0.800	1495.65	0.3327	4.33	[38]
Yb^{3+}-O^{2-}	0.868	1649.80	0.3386	16.57	[16]
Y^{3+}-O^{2-}	0.900	1766.4	0.33849	19.43	[36]
Sm^{3+}-O^{2-}	0.958	1944.44	0.3414	21.49	[16]
La^{3+}-O^{2-}	1.032	2088.89	0.3460	23.25	[7]
Rh^{4+}-O^{2-}	0.600	1204.64	0.3404	0.0	[38]
Ti^{4+}-O^{2-}	0.605	1210.04	0.3427	0.0	[38]
Ru^{4+}-O^{2-}	0.620	1215.78	0.3441	0.0	[16]
Mo^{4+}-O^{2-}	0.650	1223.97	0.347	0.0	[16]
Sn^{4+}-O^{2-}	0.790	1414.32	0.3479	13.6	[16]
Pu^{4+}-O^{2-}	0.860	1682.08	0.3542	0.0	[38]

3.3.1 Isolated Point Defect Simulations

In point defect chemistry there are two basic types of defect: vacancy and interstitial. More complex defects can be constructed from these. For example, a substitutional defect can be formed by creating a vacancy and then introducing an extrinsic interstitial into that same site. Any defect will introduce a level of strain into the lattice and the simulation will report this as a defect energy. When a reported energy refers to a single defect this is considered an *isolated* defect result. These energies can be used to evaluate reaction energies where there is no defect-defect interaction expected. However, simulations are not restricted to this scenario only.

3.3.2 Point Defect Cluster Simulations

It is possible to define several defects in one simulation. A single energy will be reported, however, in this case the energy is considered a *clustered* result. In this way the interaction of defects with each other is accounted for. Cluster formation can lead to a substantial reduction in the energy depending on geometry and the ion radii. This reduction in energy is called the binding energy, E^{bin}, which can indicate if strong defect associations will form in systems at appropriate temperatures. E^{bin} is defined as the difference in energy between the sum of the formation energies of the clusters components when they are spatially isolated, $\sum E_{defects}$, and the formation energy of the cluster, $E_{cluster}$,

$$E^{bin} = \sum E_{defects} - E_{cluster} \tag{3.39}$$

Thus, a positive binding energy indicates that a given cluster is stable. There are two components to the binding energy [40]. Firstly the coulombic interaction which is a consequence of oppositely charged defects acting to reduce the overall charge disruption in the lattice. Secondly, the lattice relaxation in which the ions move to a more favourable

geometry. For example, a vacancy close to an over-sized solute cation will reduce the overall strain in the lattice.

While it is generally found that the cooperative relaxation is only significant when defects are in close proximity, there may be many complex arrangements for the neighbouring defects, each with different energies. It is important to consider all the possible geometries so that the lowest energy (most favourable) can be predicted. This is indicated by the largest overall binding energy. The number and complexity of the clusters is purely a function of system crystallography.

Differentiating the many clusters can become difficult for a complex system, thus a consistent approach for naming clusters has been devised. The various solution geometries in chapters 4 and 5 arise form the arrangement of the substitutional defects in the 1^{st}, 2^{nd}, 3^{rd} and occasionally 4^{th} or 5^{th} neighbour sites around a compensating defect. Cluster designations are assigned based on the near neighbour position of each of the substitutional defects. Thus, a cluster containing 4 defects (1 compensating and 3 substitutional) of which two are in 1^{st} neighbour positions and one in a 3^{rd} neighbour position would be called 1-1-3. If there are several clusters with a 1-1-3 arrangement then they are differentiated by an alphabetical character. Thus: 1-1-3a, 1-1-3b, 1-1-3c and so on. Explicit coordinates of each site in the cluster are provided in the text.

While clustering is an important issue, the analysis required to fully resolve its complexity is prohibitive. For this work a simpler limiting case is used which introduced the following issues:

- The defect cluster energetics are wholly represented by the single lowest defect cluster energy configuration. As such, the contribution to the configurational entropy from the cluster configuration is ignored.

- Thus, solution reactions for the clustered case are only valid in a highly limiting case.

A fully comprehensive treatment would consider the equilibrium between the isolated and clustered cases as a means to determine the partition between the isolated and clustered defect concentrations. However, this is beyond the scope of this thesis and solution limits based on the defect cluster energies are not entirely rigorous.

3.3.3 Migration Saddle Point Energy Simulations

The bulk transport properties of intrinsic defects is also of interest as it is indicative of passivation layer stability. The simulation code can be used to calculate saddle point energies for migration pathways. Assuming that migration occurs primarily via a thermally activated hopping process, the difference between the energy of the migrating defect at the saddle point and an isolated defect represents the energy barrier to migration and is related to the activation energy. The activation energy is related to transport in the lattice as discussed in section 1.3.2. The location of the saddle point is established by compiling contour plots of defect energies between the start and end point of the migration. Assuming the migrating defect will follow the lowest energy pathway, this type of plot allows the migration path and saddle point to be identified.

In contour plots higher energies are red shades and lower energies are blue shades. Imagining this to form a three dimensional topographical surface, for a plane parallel to the migration path then the surface will look like a valley and the valley floor will describe the migration path. For a plane perpendicular to the migration path the surface will look like a sinkhole and the bottom of the sinkhole will describe a single point on the migration path. Several planes may be required to accurately locate the saddle point. Examples for these contour plots can bee seen in section 4.4.3.

In the simulations a lattice geometry is defined which represents the expected configuration at some point during the migration hop. The migrating ion is fixed and the

surrounding lattice relaxed. In figure 3.5 the schematic represents the configuration used to locate a saddle point for a vacancy migrating in a (001) direction in NiF_2. Fixed defects are rastered in a plane perpendicular to the expected path.

Since the number of calculations required for a single contour plot may be several hundred, a smaller region I size is used to decrease the computational load. Full region I size calculations are then made along the predicted migration path, the results of which can be plotted as an energy barrier graph. Examples for these energy barrier graphs can be seen in section 4.4.3. It has been found that the smaller region I size calculations give the same spatial location of the saddle point while the absolute values of the defect energies may differ from full region I size calculations.

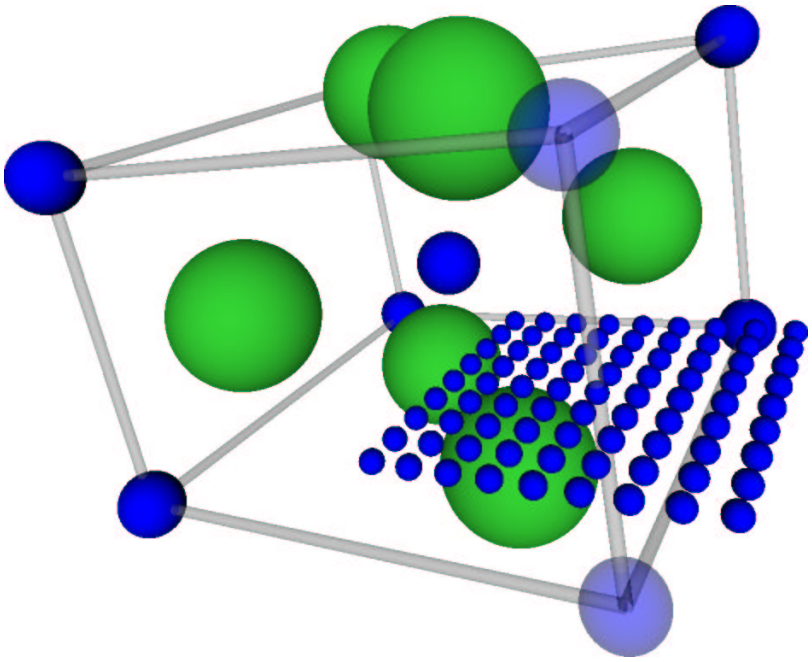

Figure 3.5: Representation of the technique used to calculate contour plot energies. This example is for a nickel vacancy migration in the [001] direction.

Migration hops can be classified by their ability to move defects through the lattice. This is dependant on what type of secondary hops are available to a defect after a primary

hop. Thus there are several possible modes of transport:

mode 1 The secondary hop is of the same type as the primary hop but results in the defect moving to a lattice site which has not previously been visited.

mode 2 The secondary hop is of the same type as the primary hop but can only result in the defect moving back to a site which was previously visited (e.g. the site from which the primary hop started).

mode 3 The secondary hop is of a different type to the primary hop and must by definition move to a lattice site which has not been previously visited.

mode 4 The secondary hop is of a different type to the primary hop but can only move the ion back to a start site that was previously visited.

A defect can only move large distances through the lattice in mode 1 or mode 3. A defect cannot move large distances through the lattice by mode 2 or mode 4. As such, mode 1 and 3 allow ‘continuous‘ migration through the lattice, and modes 2 and 4 do not. Thus, modes 2 and 4 may be considered ‘discontinuous‘.